HHS Public Access

Author manuscript

Phys Med Biol. Author manuscript; available in PMC 2023 October 20.

Published in final edited form as:

Phys Med Biol. ; 67(21): . doi:10.1088/1361-6560/ac96c7.

Mechanical damage thresholds for hematomas near gas-containing bodies in pulsed HIFU fields

Ekaterina M. Ponomarchuk[1], **Christopher Hunter**[2], **Minho Song**[3], **Vera A. Khokhlova**[1,2], **Oleg A. Sapozhnikov**[1,2], **Petr V. Yuldashev**[1], **Tatiana D. Khokhlova**[3]

[1]Physics Faculty, Lomonosov Moscow State University, Moscow, Russian Federation

[2]Center for Industrial and Medical Ultrasound, University of Washington, Seattle, United States of America

[3]Department of Gastroenterology, University of Washington, Seattle, United States of America

Abstract

Objective: Boiling histotripsy (BH) is a novel high intensity focused ultrasound (HIFU) application currently being developed for non-invasive mechanical fractionation of soft tissues and large hematomas. In the context of development of BH treatment planning approaches for ablating targets adjacent to gas-containing organs, this study aimed at investigation of the ultrasound pressure thresholds of atomization-induced damage to the tissue-air interface and correlation of the danger zone dimensions with spatial structure of nonlinear HIFU field parameters.

Approach: A flat interface with air of freshly clotted bovine blood was used as an *ex vivo* model due to its homogenous structure and higher susceptibility to ultrasound-induced mechanical damage compared to soft tissues. Three 1.5 MHz transducers of different *F*-numbers (0.77, 1 and 1.5) were focused at various distances before or beyond a flat clot surface, and a BH exposure was delivered either at constant, high-amplitude output level, or at gradually increasing level until a visible damage to the clot surface occurred. The HIFU pressure field parameters at the clot surface were determined through a combination of hydrophone measurements in water, forward wave propagation simulation using “HIFU beam” software and an image source method to account for the wave reflection from the clot surface and formation of a standing wave. The iso-levels of peak negative pressure in the resulting HIFU field were correlated to the outlines of surface erosion to identify the danger zone around the BH focus.

Main results: The outline of the danger zone was shown to differ from that of a typical BH lesion produced in a volume of clot material. In the prefocal area, the zone was confined within the 4 MPa contour of the incident peak-to-peak pressure; within the main focal lobe it was determined by the maximum BH lesion width, and in the postfocal area – by the transverse size of the focal lobe and position of the first postfocal pressure axial null.

Significance: The incident HIFU pressure-based danger zone boundaries were outlined around the BH focus and can be superimposed onto in-treatment ultrasound image to avoid damage to adjacent gas-containing bodies.

ponomarchuk.em14@physics.msu.ru .

Keywords

HIFU; non-invasive surgery; mechanical tissue ablation; boiling histotripsy; hematoma liquefaction; ultrasonic atomization

1. Introduction

A number of approaches to non-invasive mechanical ablation of tissues using high amplitude bursts of HIFU – histotripsy – have been developed as an alternative to thermal ablation techniques using high-intensity focused ultrasound (HIFU) (Maxwell et al 2012, Khokhlova V A et al 2015). One of the histotripsy types termed boiling histotripsy (BH) utilizes relatively long HIFU pulses of several milliseconds containing shock waves at the focus due to nonlinear propagation effects delivered with a low duty cycle of about 1–2% to eliminate thermal effects (Khokhlova et al 2011). Rapid localized shock wave superheating leads to elevation of tissue temperature up to 100°C within each pulse and interaction between the ensuing vapor bubbles and incident shock waves leads to tissue mechanical fractionation to a liquid state (Maxwell et al 2012, Simon et al 2012).

A typical single BH lesion consists of an ellipsoidal cavity located prefocally, usually called the “head”, and a thinner elongated postfocal part, called the “tail” (figure 1(a)). The “head” is believed to form by a combination of several effects: cavitation in front of the vapor bubble induced by the formation of a localized large negative pressure region when high-amplitude shock waves reflect from the tissue-vapor pressure-release interface, detachment of tissue fragments into the vapor cavity through direct spallation mechanism, formation of a miniature acoustic fountain at the proximal surface of the cavity – a jet of debris in direction of the incident wave propagation, and the loss of stability of the surface of this jet with the separation of small tissue fragments (the effect of acoustic atomization) (Simon et al 2012, 2015, Pahk et al. 2019, 2021). Since the result of all these interrelated processes in BH exposures is the breakdown of tissue into subcellular fragments they will collectively be referred to here as atomization for brevity. One of the proposed mechanisms for the formation of the BH lesion “tail” is the aforementioned jet of atomized tissue inside the vapor cavity, generated by the radiation force of the superfocused HIFU beam of submillimeter diameter. This high-speed jet emerges from the proximal surface of the vapor cavity and impinges on the opposite (distal) surface, thus creating a channel in tissue – the “tail” (Khokhlova et al 2017). An alternative explanation for the “tail” formation is the appearance of secondary vapor bubbles behind the first one due to diffraction of the incident HIFU field around it (Pahk et al. 2019).

BH is currently being developed for a number of clinical applications, including mechanical tumor ablation, disinfection of abscesses, and liquefaction of large hematomas for subsequent fine needle aspiration (Khokhlova et al 2016, Ponomarchuk et al 2021, Matula et al 2021). All of those ablation targets are frequently located in the abdominal cavity, in the immediate vicinity of gas-containing organs, such as stomach, intestines, and lungs. HIFU waves incident on an interface of a gas-containing organ is known to carry an increased risk of mechanical damage to the interface tissue through atomization at the pressure-release

interface (Li et al 2007). The exact subsurface pressure threshold of damage to the wall of an air-filled organ is not known, and keeping HIFU pressures below this threshold is especially important for high-amplitude pulsed exposures like BH.

Thus, the mechanisms involved in the interaction of high-amplitude ultrasound waves with a pressure-release interface determine, firstly, the shape and size of the BH lesions and, secondly, the damage threshold for gas-containing organs adjacent to the lesion. Both of these aspects are essential for treatment planning. The overall goal of this work in the context of BH liquefaction of large intraabdominal hematomas, was to relate the ultrasound field parameters to the two aforementioned treatment effects: the BH lesion dimensions and the danger zone around the focus beyond which the interface with gas-filled organs will not be damaged (figure 1(b)).

The shape and size of a single BH lesion depend on the transducer parameters (frequency and focusing angle), pulse duration, tissue mechanical properties, and the duration of treatment, i.e., the number of BH pulses delivered. Across all the transducer parameters, pulse durations, and target tissues (e.g. bovine blood clots, liver and cardiac tissue), the BH lesion size was reported to increase with the number of delivered BH pulses before reaching saturation within 5–20 pulses. The specific number depended on the tissue mechanical properties and pulse duration (Khokhlova et al 2011, 2016, 2018a, Simon et al 2012). Decrease in the operating frequency of the BH transducer has also been shown to result in increased size of the BH lesions, leading, however, to a higher probability of detrimental prefocal cavitation shielding the focal region at frequencies below 1.2 MHz (Khokhlova et al 2011, 2017). The abovementioned exposure parameters have also been extensively studied by Vlaisavljevich et al (2015a, 2015b, 2017) in the context of other histotripsy techniques as well.

It has also been shown in the bovine blood clots that the increase in the focusing angle of a BH transducer leads to a more rounded (i.e. wider in lateral dimension and shorter axially) “head” of the BH lesion, and a narrower and shorter lesion “tail” (Khokhlova et al 2018a).

The type of the target tissue, specifically its elastic modulus and toughness, strongly affect the shape and size of the BH lesion (Khokhlova et al 2011, 2014, 2018a, 2020, Simon et al 2012, Wang et al 2013, 2018, Khokhlova V A et al 2015). Connective tissues with high collagen content have been reported to have the highest resistance to mechanical destruction by BH (Khokhlova et al 2014, Wang 2018), whereas blood clots are the most sensitive (Simon et al 2012, Khokhlova et al 2016). Accordingly, the thresholds for ultrasound atomization of tissue – one of the mechanisms mediating BH – were also found to be dependent on the tissue type. Simon et al (2012) reported on the threshold intensity of HIFU required for atomization of bovine liver and porcine blood clots, with the focus positioned at the planar tissue-air interface. The threshold intensity for atomization of porcine blood clots was found to be lower than that for bovine liver tissue.

Highest sensitivity of blood clot material to atomization-induced mechanical damage among all other soft tissues suggests that it may serve as a good model for investigating the risk of damage to gas-filled organs adjacent to the BH treatment site. Specifically, if no mechanical

damage occurs to a clot-air interface present within the HIFU beam during BH exposure, then no such damage would be expected to a similarly positioned surface of a gas-containing organ because of its greater resistance to atomization. In other words, the large clot-air interface represents the worst-case scenario model of a wall of a gas-containing organ in terms of collateral damage during BH treatment in adjacent tissue.

The above arguments led us to select large volume bovine blood clots as an *ex vivo* model to study the dependence of the BH lesion shape and size on HIFU field parameters and to determine the boundary of danger zone around the focus, outside of which the risk of damage to a gas-containing organ is minimal. In addition, unlike most soft tissues, the large volume clot material was found to be remarkably homogenous, and its mechanical properties very consistent and repeatable, thus reducing tissue-based variability in results (Khokhlova et al 2020).

The study described here consisted of two parts. In the first part, the influence of the transducer focusing angle (or *F*-number) and a planar clot-air interface position relatively to the HIFU transducer focus on the result of a typical BH exposure was investigated. Three HIFU transducers with different *F*-numbers were used to deliver a typical BH exposure, with the focus positioned at controlled distances before or beyond the interface. The outlines of the resulting BH lesions and surface erosion were compared to the iso-pressure levels of the numerically simulated parameters of the corresponding HIFU fields to determine the pressure thresholds of damaging a pressure-release interface. Note that two different mechanisms are expected to be responsible for the surface damage when focusing before or beyond the interface. When the focus is placed inside the clot volume, before the surface, the standard BH processes occur. Vapor bubbles and cavitation clouds forming at the focus block the HIFU field partially or completely, and thus prevent the atomization of the surface located postfocally. However, the high-speed jet of liquified material associated with the acoustic micro-fountain mechanism during BH impinges on the distal side of the gas/vapor cavity creating a tunnel towards the surface and facilitating surface damage. Conversely, when the focus is positioned outside the sample, beyond the clot-air interface, the primary mechanism of surface damage will be direct atomization by the HIFU field.

In the second part, the influence of the transducer focusing angle on clot surface atomization threshold was investigated for different focus positions before or beyond the surface. The same three transducers were used to deliver single pulses with duration typical for BH to the clot sample, with the focus being located at controlled distances before or beyond the clot-air interface. The HIFU output level was increased until visually observable damage to the clot surface occurred, and the corresponding output level was defined as the threshold. Based on the HIFU field hydrophone measurements and modeling, this threshold was then related to the corresponding maximum negative pressure *in situ*.

The thresholds determined from the first and second parts of the study were then compared to determine danger zone around a BH transducer focus.

2. Materials and methods

2.1 In vitro hematoma model

Fresh bovine blood was obtained from local abattoir, anticoagulated with citratephosphatedextrose (CPD, No. C7165; Millipore-Sigma, St. Louis, MO, USA) at a 9:1 volume ratio, kept refrigerated at 5°C, and used for experiments within a week. At the day of each experiment, anticoagulated blood was poured into rectangular plastic molds with 5×5cm base, de-gassed at room temperature for 60–70 min and coagulated by adding 25 mmol/L of $CaCl_2$ solution (No. C3306, Millipore-Sigma). The height of the clot samples varied from 2 to 4 cm depending on the focusing angle of the transducer used for each sample and the expected focus position. Prior to sonication, the sample was placed into a plastic mold with an acoustically transparent bottom, attached to a 3-D positioning system and partially immersed in a tank with filtered and de-ionized water which was preliminary de-gassed for 60–70 min. The bottom horizontal side of the clot was placed in water, and the upper side contacted with air (figure 2(a,b)).

2.2 Experimental setup and procedures

The experimental setup is illustrated in figure 2(a,b). Three 1.5 MHz HIFU transducers (figure 2(c)) with the same apertures but different *F*-numbers (ratio of the focal length and aperture) – 0.77, 1 and 1.5 were used (Khokhlova et al 2018b). Nominal parameters of the transducers are listed in table 1. The transducers were driven by a custom-built class D amplifier with the input waveform generated by a computer-controlled field-programmable gate array (FPGA) board (Maxwell et al 2017).

The HIFU transducers had a central opening that incorporated a 5 MHz focused transducer with 13 mm aperture and 63 mm radius of curvature (Olympus NDT) that worked as a pulse-echo probe controlled by a pulser-receiver (Panametrics PR5072, Waltham, MA, USA) and a digital oscilloscope (DSO-X 3034A, Keysight Technologies, Inc., Santa Rosa, CA). The pulse-echo measurement was used to control the distance between the HIFU focus and the clot-air interface. The HIFU focus was defined as the point of maximum peak positive pressure in the shock-forming regime in free field. The time delay corresponding to the focus was pre-recorded during hydrophone characterization of the transducers in free field. The correction to that delay introduced by the presence of the clot layer in the ultrasound path was accounted for based on the thickness of the hematoma sample and the sound speed in water (c_w = 1500 m/s) and in bovine blood clot, which was measured in n=6 clot samples using acoustic calipers (c_c = 1560±20 m/s) (Hunter et al 2016). Positioning of the HIFU focus relative to the clot-air interface was achieved by mechanical translation of the clot sample in axial direction by a 3D-positioning system (Velmex, Inc., Bloomfield, NY). The step between focus positions was 1 mm for *F*# = 0.77 and *F*# = 1 transducers, and 2 mm for *F*# = 1.5 transducer. Each position was repeated n = 1–3 times. In the first series of experiments the HIFU exposure parameters (table 1) typical for BH in soft tissues (10–20 ms pulses with 1–2% duty cycle) were used that corresponded to the fully developed shock regime so that tissue boiling at the focus was achieved within each pulse (Khokhlova et al 2011, 2014, 2016, Simon et al 2012, Wang et al 2013, Khokhlova V A et al 2015). Evaluation of the time-to-boil (t_b) is described in section 2.4. The acoustic power (W_0), peak

focal pressures, and shock amplitude *in situ* (P_+ / P_- / A_s) were determined from combined hydrophone measurements and simulations described in section 2.3. The number of BH pulses delivered per exposure corresponded to the saturation of the BH lesion size for the chosen pulsing protocol (Khokhlova et al 2016, 2018a). The initiation of bubble activity inside the clot was confirmed by the pulse-echo probe. The HIFU focus was positioned either before the clot-air interface, at a depth ranging from zero to a distance that allowed producing a BH lesion fully inside the sample, L_{before}, or beyond the interface ranging from zero to a distance that did not result in any visually discernable damage to the clot surface, L_{beyond} (figure 2(d)). Following a BH exposure, the clot-air planar interface of the sample was photographed, then the sample was bisected vertically along the HIFU axis, and the cut surface was also photographed to obtain the outline of the lesion in 3D. At least n=3 lesions per focus position for a given HIFU transducer were produced to test the variability of the results. Note that prior to BH exposure the clot surface was not perfectly flat and inevitably had some surface undulations shallower than 1 mm (e.g. the surface seen in Fig.2b). Thus, surface defects found after the BH exposure that were comparable in size and depth to pre-existing ones were challenging to discern visually and unambiguously attribute to the exposure. Given this limitation, the defects less than 1 mm in depth and diameter were referred to as absence of damage to the clot surface.

In the second series of experiments, the HIFU focus was also positioned at controlled distances before or beyond the clot-air interface, and the same HIFU transducers delivered isolated pulses of the same duration and duty cycle as those in table 1, but with output power gradually increasing until a visually discernable damage to the surface was generated via acoustic atomization. The corresponding *in situ* pressure fields were determined from the combined measurement and modelling approach and considered as the atomization threshold.

To compare the atomization threshold in the blood clot with that in water, where atomization is more thoroughly studied (Rozenberg and Eknadiosyants 1960, Tomita 2014, Simon et al 2015, Gaete-Garretón et al 2018, Aikawa and Nobuki 2021, Kim et al 2021), the same experiment was conducted for a de-gassed water surface but the threshold pressures were defined as those resulting in visually discernable detachment of a water droplet.

2.3 HIFU field characterization

The HIFU fields inside blood clots during all exposures were simulated using “HIFU beam” software (Yuldashev et al 2021). The boundary conditions for all three transducers were set from hydrophone measurements following an equivalent source approach (Canney et al 2008, Khokhlova et al 2018b, Khokhlova V A et al 2018).

2.3.1 Hydrophone measurements in water.—

Two series of the hydrophone measurements were performed in a tank filled with de-gassed water.

First, axial pressure distributions were measured in the low-output (linear propagation) regime using a 200 μm aperture calibrated capsule hydrophone (HGL-0200 with AH-2020 preamplifier, Onda Corp., Sunnyvale, CA). These measurements were used to define the parameters of the equivalent source for each HIFU transducer (aperture, focal length, and

size of central opening). Absolute values of the measured pressure amplitude were used to obtain the pressure amplitude at the transducer surface, p_0, and relate it to the corresponding HIFU driving voltage amplitude, V. The ratio p_0/V was used in "HIFU beam" simulations performed at increased driving voltage.

Second, to confirm the results of numerical simulations of the high-amplitude fields of the equivalent sources with parameters determined above, a set of focal pressure waveform measurements over the full scale of output levels was performed in water using a fiber-optic probe hydrophone (FOPH2000, 100μm fiber tip diameter, 100 MHz bandwidth, RP Acoustics, Leutenbach, Germany). As stated earlier, the focus was defined as the location of the maximum peak positive pressure found at a shock-forming output level. The measured focal waveforms were postprocessed to determine the dependence of peak positive and negative focal pressures on the transducer driving voltage.

2.3.2 Numerical simulations in water. —The calculations of the HIFU fields were performed using a simulator "HIFU beam" for modeling of linear and nonlinear fields generated by axially symmetric HIFU transducers based on wide-angle parabolic representation of the Westervelt equation (Khokhlova V A et al 2018, Yuldashev et al 2018, 2021). The simulator is available for download at http://limu.msu.ru/node/3555?language=en. First, the parameters of the equivalent source in the simulation were varied close to the nominal ones to achieve the best match between the measured and modeled axial pressure distributions in the linear regime in water. The resulting set of equivalent source parameters was then used as a boundary condition for nonlinear propagation modeling.

High-power field calculations were performed with the pressure amplitude at the surface p_0 of the equivalent source increasing proportionally to the experimentally increased source driving voltage V, and the saturation curves at the focal point were obtained and compared to the hydrophone measurements. The equivalent source parameters obtained for each of the three transducers were then used for modeling of the 3D nonlinear fields produced in the hematoma models for each position of the HIFU focus relative to the air interface.

2.3.3 Numerical simulations in hematoma sample. —The acoustic parameters of the bovine hematoma required for numerical field calculations were taken from the literature as follows: hematoma density $\rho = 1060$ kg/m^3, nonlinear parameter $\beta = 4$, exponent in the absorption power law $\nu = 1.1$ (Grybauskas et al 1978, Duck 1990, Nahirnyak et al 2006, Khokhlova et al 2016). Longitudinal wave velocity $c_1 = 1560$ m/s and attenuation coefficient at 1.5 MHz $\alpha = 0.045$ Np/cm were measured using acoustic calipers and insertion method. The diffusivity of sound was taken as its standard value for water: $\delta = 4.33$ mm^2/s.

The propagation medium used in the simulations was considered consisting of two flat layers – a water layer and a semi-infinite layer of clotted blood with the boundary shifted in each simulation depending on the focus position relative to the clot layer.

Wave reflection from the air-clot surface and standing waves formation inside the clot were accounted for by an image source approach (Pierce 2014): the pressure-release boundary condition at the clot–air interface was provided by introducing an imaginary mirror source

emitting an inverted wave in the direction opposite to the real source. The superposition of waves from two mirrored sources provided zero pressure at the interface, and the interference of these counterpropagating waves near the clot surface led to the formation of a quasi-standing wave.

2.4 Evaluation of time-to-boil and tissue displacement due to radiation force

According to Khokhlova et al (2011) and Canney et al (2010), when the heating rate at the focal spot of the beam is high enough for boiling to occur within several milliseconds, the thermal diffusion is negligible and the time for tissue to reach boiling at the focus can be evaluated as follows:

$$t_b = \frac{\Delta T \mathrm{c}_v}{H} \quad (1),$$

where ΔT is the temperature change from the ambient to the tissue boiling temperature 100 °C, c_V is the tissue heat capacity per unit volume, H is the heating rate of the medium. The heat capacity per unit volume of the bovine coagulated blood c_V was evaluated as the average between the values for human and porcine blood clots: c_V = 3.5 MJ/m^3·K (Nahirnyak et al 2006). The heating rate H was determined from the numerical simulations as the maximum heating rate value within the focal lobe with the focus positioned at the average experimental depth in the clot layer for each transducer (17, 20 and 25 mm for $F\#$ = 0.77, 1.02 and 1.51, respectively) and was as follows: H_{max} = 300.2, 158 and 25.6 kW/cm^3 for corresponding ultrasound sources. The evaluated values of the time-to-boil for each transducer are listed in table 1.

The radiation force induced in tissue by the HIFU beam causes tissue displacement along the beam axis which then results in shear wave propagation in transverse direction (Andreev et al 1997, Pishchalnikov et al 2002). The maximum value of this displacement over time within the HIFU pulse depends on the amplitude of the radiation force per unit volume F_0, characteristic transverse beam radius a and the tissue shear wave velocity c_t. Taking the approximation of the transverse distribution of the axial component of the radiation force as

$$F(r) = \frac{F_0}{\left(1 + \frac{r^2}{a^2}\right)^{3/2}}, \quad (2)$$

the tissue displacement can be evaluated as follows:

$$u(t) = \frac{F_0}{2}\left(\frac{a}{c_t}\right)^2 \ln\left\{1 + \left(\frac{c_t t}{a}\right)^2\right\} \quad (3)$$

(Andreev et al 1997, Pishchalnikov et al 2002, Poliachik et al 2014). The radiation force amplitude F_0 is defined by the peak heating rate in the HIFU beam H_{max} and the tissue properties:

$$F_0 = \frac{H_{max}}{\rho c_l}. \tag{4}$$

(Sapozhnikov 2015, Prieur et al 2017). The effective radius of the radiation force localization area was evaluated based on the equality of the cross-sectional integrals of normalized distributions of the radiation force $F(r)/F_0$ and the heating rate $H(r)/H_{max}$:

$$\int_0^\infty 2\pi r dr \frac{H(r)}{H_{max}} = \int_0^\infty 2\pi r dr \frac{F(r)}{F_0} = 2\pi \int_0^\infty \frac{r dr}{\left(1+\frac{r^2}{a^2}\right)^{3/2}} = 2\pi a^2, \tag{5}$$

and thus was calculated as follows:

$$a = \sqrt{\int_0^\infty r dr \frac{H(r)}{H_{max}}}. \tag{6}$$

The shear wave speed in the bovine coagulated blood was calculated as

$$c_t = \sqrt{\frac{\mu}{\rho}}, \tag{7}$$

where ρ is the clot density and μ is its shear modulus which was 0.95 kPa as measured by the indentometer method described by Waters (1965) and Khokhlova et al (2020).

2.5 Correlation of surface erosion with the ultrasound field parameters

All atomization-induced surface erosions were photographed at the surface and in bisection along the HIFU transducer axis. The erosions were shaped as circular wells with characteristic depth and diameter. These dimensions were measured with a ruler for each focus position and compared to the simulated 2D distributions of peak positive and negative pressures in the standing wave field. For the cases when the HIFU focus was positioned in the air, i.e. beyond the clot surface, the modeled incident field was numerically reflected from the pressure-release surface corresponding either to the bottom of the atomization-induced lesion or, if no lesion occured, to the surface of the clot. The maximum value of the peak negative pressure in the resulting quasi-standing wave field was determined in a λ/4-thick subsurface layer, i.e. a layer including the first maximum of the standing wave. The map of thus determined modeled peak negative pressure was superimposed on the outline of the experimentally measured surface erosions. The peak negative pressure at the erosion rim was determined as the damage threshold. The uncertainty of the threshold caused by the erosion depth and width measurement error (0.5 mm) was determined by varying the erosion dimensions within that error. Note that these correlations were not performed for the cases where the HIFU focus was positioned before the surface of the clot, i.e., when the vapor bubbles formed in the clot at the focus. In these cases the postfocal HIFU field would have been severely distorted or completely blocked by the vapor bubble and prefocal cavitation clouds, precluding any meaningful correlations.

In the second set of experiments involving lower-amplitude atomization at the clot or water surface, the maximum value of peak negative pressure was determined in a 2λ-thick layer under the planar clot-air interface. A thicker subsurface layer for lower-amplitude simulations compared to higher-amplitude ones was used due to a larger size of the focal lobe at lower intensities and, therefore, larger scale of acoustic pressure changes. The values of uncertainty were calculated based on the 10% inaccuracy of the output voltage adjustment and its relation with the peak pressure according to the saturation curves.

3. Results

3.1 Transducer field characterization

Figure 3(a,b) shows good agreement between the measured pressure amplitude axial scans in the linear regime and those modelled with the best fit geometrical parameters of the equivalent sources. The parameters of the equivalent sources are compared to the nominal ones in table 2.

The ratio p_0/V was determined by matching the experimental saturation curves with the simulated ones primarily in quasi-linear regimes (figure 3(c)) as the experimentally measured peak pressures at higher outputs can be underestimated due to the limited size of the hydrophone sensitive area comparable to the width of the nonlinear focal lobe. The acoustic output power W_0 was calculated from the transducer surface pressure p_0, sound speed in water c_0, its density ρ_0 and surface area S of the transducer listed in table 2 as follows: $W_0 = \frac{p_0^2}{2\rho_0 c_0} \cdot S$.

3.2 Tissue displacement evaluation

The tissue displacement over time evaluated by the Eq. 3 for each of the three transducers is depicted in figure 3(d) and, within the time-to-boil, was 2, 4.5 and 3.6 mm for transducers with F-numbers 0.83, 1.13 and 1.6, respectively.

3.3 Lesion analysis

Figure 4 illustrates representative examples of the surface damage (top row) and its axial bisections (bottom row) for the transducer with $F\#$ = 1.13 for focus positions before the clot-air interface (figure 4(a)) and beyond the clot-air interface (figure 4(b)) up to the distances at which no damage is caused to the surface. These prefocal and postfocal distances will be referred to as “safe distances”.

The safe distances for each transducer are provided in table 3 and were shown to increase for weakly focusing transducers.

When the focus was positioned inside the sample, and boiling was initiated, the surface damage disappeared at smaller distances (L_{before}) than it did when focus was positioned beyond the sample and surface atomization occured (L_{beyond}). For the source with the highest F-number ($F\#$ = 1.6), the safe distance for the focus inside the clot was shown to be more than 16 mm but was not precisely determined experimentally due to a large thickness

of the hematoma required to produce a full-sized BH lesion at a significant depth of the focus under the surface (Khokhlova et al 2018a).

As seen in figure 4(a), when the HIFU focus was positioned before the clot-air interface, the BH lesions inside the samples (bottom row) were tadpole-shaped, typical for BH and indicating that the surface damage was generated by acoustic streaming of the fractionated tissue fragments, i.e., by the “tail” of the BH lesion. This was also supported by the circular shape of the surface damage induced by the jet (figure 4(a), top row) as opposed to the more irregular shape of the surface erosion caused by acoustic atomization (figure 4(b), top row, middle panel).

The shape of the lesion was also shown to depend on the transducer *F*-number (table 3). When the focus was positioned inside the sample, the HIFU transducers with higher *F*-numbers generated narrower and more axially elongated boiling-induced “tadpole”-shaped lesions of larger diameter at the sample surface. When the focus was positioned beyond the sample surface, the atomization-induced lesions were deeper for higher *F*-numbers, whereas the surface erosion decreased in diameter.

Figure 5 illustrates correlation between the average diameters of the observed surface damage (diameter *d* in figure 2(d)) and typical BH lesions produced inside a large clot sample, far from its boundaries. The prefocal danger zone outline in axial direction (red crosses on the left of each picture) is positioned much more prefocally relatively to the “head” of a typical BH lesion, whereas postfocally the safe distance is smaller than the length of the “tail”. Within the main focal lobe, the surface erosion diameter is close to the width of the BH lesion “head” and is also larger than the average width of the surface damage $<d>$ when the surface was located outside the focal lobe. As seen on the background photographs in figure 5, the “tails” of the in-bulk lesions produced by $F\# = 0.83$ and 1.13 transducers were curved which has been observed previously (Khokhlova et al 2016). We attribute this effect to inhomogeneity in fibrin matrix structure specific to each particular clot sample, which defines resistance of the clot material to the tissue streaming of tissue fragments during the “tail” formation.

3.4 Correlation of the BH lesions with the HIFU fields

As seen in table 3, the postfocal safe distance (L_{before}), i.e., when the focus is inside the clot, is close to the distance from the focal point to the first postfocal pressure axial null in numerically simulated linear field (Δz_{post}), whereas the prefocal safe distance (L_{beyond}), i.e. when the focus is beyond the clot surface, is over 2-fold larger than the distance to the first prefocal pressure null (Δz_{pre}). This distance Δz_{pre}, however, correlates with the average length of the BH lesion “head” ($<l>$) which is in agreement with the results for the BH lesions produced within a clot volume (Khokhlova et al 2018a, 2020). The width of the BH lesion “head” did not correlate with any field parameters. The average diameter of the surface damage $<d>$ when HIFU focus was inside the clot but the surface was outside the focal lobe was observed to correlate with the width of the focal lobe and the average diameter of the BH lesion “tail” $<D>$. For the weakest-focusing transducer, the average diameter of the jet-induced damage at the surface was larger than the width of the “tail” and of the focal lobe (table 3). We speculate that this may be because the surface

was still located within the focal lobe even at the furthest considered distance from the focus and, therefore, was damaged not necessarily by the “tail”-forming jet but also by the “head”-forming mechanisms.

Figure 6 shows a representative example (a–c) and summarized results (d) of surface erosion shape correlation with the pressure field of nonlinear standing wave induced inside hematomas when focus was positioned beyond the surface. The outlines of the surface erosions were observed to lie within 4 MPa contour of the peak negative pressure at the erosion bottom. This is demonstrated both by superimposition of the surface lesions onto the standing wave field (Fig. 6a–c) and by surface erosion radii being lower than corresponding 4 MPa peak negative pressure radii (Fig. 6d). This value of peak negative pressure in the standing wave in this case also corresponded to the 4 MPa contour of the peak-to-peak pressure in the incident acoustic field. These pressure values were considered as thresholds for atomization-induced damage.

The atomization threshold values for the negative pressure determined from correlation of BH lesions with HIFU fields for all focus positions beyond the clot surface are summarized in figure 7(a). As seen, the threshold values were observed to be dependent on the focus position relative to the pressure-release interface and were generally higher for the focus positions within 10 mm of the surface. We speculate that this discrepancy may be in part due to the strong distorion of the surface by the acoustic radiation force when it is within the focal region and the formation of a mound which has been observed by Simon et al (2012) to have a focusing effect on the reflected wave. While the exact height of the mound was not measured here, the calculated axial shift of bulk tissue due to radiation force, which was highest, at 4.5 mm, for the medium-focusing transducer and lowest, at 2 mm, for the most-focusing transducer, provides some indication of values that may be expected. Furthermore when the focus was positioned in close proximity to the surface (up to 4 mm), formation of vapor bubbles within the axially displaced tissue was detected by the US sensor (asterisk markers in figure 7(a)) and, therefore, represented the BH-induced surface damage rather than atomization-only based damage. The numerical simulations of the incident HIFU field and standing wave formation were performed for a planar and stationary clot-air interface and may thus provide erroneously variable and elevated values for the threshold. The atomization threshold values, therefore, were defined as the lowest P_- values causing damage to the hematoma surface over the entirety of focus positions (dashed box in figure 7(a)). These values were similar for all three transducers and ranged within 4–6 MPa.

The atomization threshold values determined from low-amplitude experiments are presented in figure 7(b). As seen, similarly to the high amplitude case, the threshold was highly dependent on the position of the focus relatively to the clot surface, and for the two transducers with lower F-numbers this dependence had a well defined maximum. The maximum corresponded to the position of the focus exactly at the surface, and the dependence flattened out at distances from the focus exceeding the length of the focal lobe (indicated for each transducer by horizontal lines at the top of figure 7(b)). We speculate that this dependence may again be caused by the elevation and curvature of the clot surface by the radiation force. Thus, the threshold measurements were considered

only for clot surface positions outside the focal lobe (dashed box in figure 7(b,c)). These threshold peak negative pressures were found to be within 3–6 MPa, similarly to the high-amplitude measurements in clot, correlating with the P_{-} = 4 MPa contour defined above. For the weakest-focusing transducer, the measured threshold values do not exhibit the same behavior and are substantially higher than those for the other two transducers at the large distances. However, note that the farthest positions of the surface from the focus were still within the focal lobe, and the mound formation could have affected the pressure levels generated under the surface. Therefore, the low-amplitude threshold for the $F\#$ = 1.6 transducer was not defined.

The measured atomization thresholds at the water-air interface showed lower threshold pressures compared to those in the hematoma (figure 7(c)). Similarly to the clot-air interface, the atomization thresholds for the two sources with lower F-numbers were shown to be dependent on the focus position relative to the water surface within the range corresponding to the focal lobe length. When the water surface was located outside the focal lobe, the dependences flattened out within 1–1.5 MPa range. Conversely, for the transducer with the highest F-number, the threshold pressure in water was remarkably independent of focus position and averaged at 1.1 MPa, consistently with the two other transducers.

3.5 Danger zone outline around the BH focus

The overall danger zone for the pressure-release interface to be near the BH focus was determined by the average dimensions of the obtained lesions and can be outlined based on the structure of the acoustic field and the typical dimensions of an in-bulk BH lesion (figure 8). Based on the results in figures 6–7, the danger zone outline in the prefocal area can be followed along the peak negative pressure contour of 4 MPa in the standing wave corresponding to the incident peak-to-peak pressure of 4 MPa. According to the results in figure 5 and table 3, the danger zone outline within the main focal lobe was determined by the maximum width of the typical BH lesion, and in the postfocal area – by the transverse width of the focal lobe and position of the first postfocal pressure axial null. As the critical distance for the weakest focusing transducer ($F\#$ = 1.6) was not determined but was shown to be more than 16 mm, the danger zone outline was assumed to follow the focal lobe width and the first postfocal pressure axial null based on the pattern observed for the other two transducers (dashed line in figure 8).

4. Discussion

The overarching goals of the study were to establish a relationship between the 3D HIFU pressure field parameters and the dimensions of the BH lesions and the danger zone outline around the HIFU focus for boundaries of gas-containing organs representing a pressure-release interface. To achieve those goals, we have generated and analyzed the BH lesions in large bovine blood clots using three HIFU transducers with varying F-numbers. The HIFU focus was positioned at varying distances from clot-air interface and the size and shape of surface erosion resulting from a typical BH exposure were examined. The BH lesions and surface erosion profiles were compared to the 3D HIFU pressure fields numerically simulated for each hematoma sample and each focus position. These analyses allowed to

both identify the minimum pressure values resulting in atomization-induced erosion of the clot material and get a deeper understanding of the process of BH lesion formation. The large clot model was selected for these experiments as the worst-case scenario, given that it is known to be more susceptible to mechanical damage than soft tissues, as well as its relevance to BH treatment of abdominal hematomas frequently located in the immediate proximity of gas-containing organs.

When the HIFU focus was located at least a few millimeters before the sample surface, i.e., inside the sample, the typical BH lesions were formed *via* previously investigated mechanisms that included reaching the boiling temperature and formation of a vapor bubble at the focus within a few milliseconds (detected here by the ultrasound sensor in the central opening of the HIFU source), excitation of prefocal cavitation which can both disrupt tissue directly and intensify tissue atomization at the pressure-release boundary of the vapor bubble and, finally, acoustic jet of the bubble remnants and atomized tissue debris away from the transducer (Simon et al 2012, Pahk et al. 2019, 2021). We have shown that the clot surface erosion in this scenario increased in diameter for transducers with higher *F*-numbers (i.e., less focused). The erosion diameter coincided with the average width of the “tail” of a typical in-bulk BH lesion and correlated to the width of the HIFU focal lobe where the radiation force pushing the tissue fragments is localized (table 3). These findings indicate that if boiling is initiated proximally to the tissue-air interface, the surface can be damaged by the atomization-induced jet of the fractionated material, similarly to the formation of the “tail” of the BH lesion (Simon et al 2012).

The BH lesion itself was overall shown to elongate and narrow with the increase in the source *F*-number. The length of the “head” was limited by the position of the prefocal axial null of the pressure field, which is in agreement with the results previously reported for BH lesions generated within the bulk of large clots (Khokhlova et al 2018a, 2020). The width of the BH lesion “head” could not be linked to any field parameter. This finding was not surprising as the “head” of the BH lesion has been previously reported to increase and saturate with increasing pulse duration and number of pulses per point at a fixed output power, i.e., with a fixed ultrasound field (Khokhlova et al 2011, 2016, 2018a, Simon et al 2012, Ponomarchuk et al 2021). The saturated width of the BH lesion “head” has been shown to depend on the target tissue and was previously reported for few tissue types.

The length of the lesion “tail” also increased for transducers with higher *F*-numbers. In considering the atomized debris jet as the mechanism for “tail” formation, this would imply that the ejected debris travel with higher velocity in the case of less focused transducers. This seemingly contradicts the results reported by Simon et al (2012) that the velocities of the tissue fragments ejected from tissue-air interface were independent of the tissue type or transducer *F*-number, and were determined by the particle velocity within the incident acoustic wave. However, the particle ejection is expected to be more omnidirectional for transducers with lower *F*-numbers, and the average axial component of that velocity is therefore lower and could arguably account for shorter lesion “tails”. Contrary to the expectations based on the dimensions of a typical in-bulk BH lesion where the “tail” usually exceeds the limits of the focal lobe, the surface here was not damaged when positioned at the first postfocal pressure axial null. One possible explanation for this effect is the presence

of surface tension at the clot-air interface that restrains the debris jet, unlike the situation in the bulk of the clot. The implication for BH treatment planning that stems from this observation is that the HIFU focus should be placed proximally to an air-filled organ at a distance equal to or larger than the distance to the first postfocal null to avoid the risk of mechanical damage.

When focus was placed outside the clot volume but close to the clot-air interface (at a distance less than 4 mm), the boiling could still be initiated due to the displacement of tissue at the focus by 3–4 mm by acoustic radiation force (figure 3). If the focus was placed further outside the sample so that boiling did not occur, the BH lesion was not produced and the hematoma surface was disrupted directly by the ultrasonic atomization. The surface erosion profile was deeper and narrower for the transducers with higher *F*-numbers. These surface erosions were confined within the contour of 4 MPa peak negative pressure in the reflected quasi-standing wave which can also be outlined by the 4 MPa peak-to-peak pressure contour in the incident wave which is more convenient for the treatment planning. Somewhat unexpectedly, this contour is substantially larger than the typical in-bulk BH lesion whose “head” in the axial dimension is limited by the first prefocal axial pressure null. These results imply that the pressure-based threshold for atomization at a planar pressure-release interface differs from that at a curved surface of a gas/vapor cavity generated by the HIFU beam during BH.

Since typical BH transducers and their acoustic fields are axially symmetric, the obtained lesions and the resulting danger zones in this study were considered axially symmetric, as well. Thus, the 3D danger zones, i.e., the outlines of the volume within which tissue-air boundaries should not be present to avoid damage to them, can be obtained by rotation of the contours in Fig. 8 about the HIFU axis. If any damage were to happen at the tissue-air boundary, it would be confined within the circular cross-section of this 3D danger zone.

The atomization threshold of 4 MPa peak-to-peak pressure in the incident HIFU wave determined from high-amplitude BH exposures and the corresponding large-scale clot surface erosion described above was also compared to that determined from lower-level exposures sufficient for generating a pinhole-sized surface erosion (figure 7).

These lower-level exposure-based threshold values fluctuated depending on the distance between the focus and the surface for all three transducers which may be attributed to the formation of a mound due to acoustic radiation force at the clot surface observed previously by Simon et al (2012). Reflection of the HIFU beam from the curved mound-air interface and refocusing below the mound can increase the effective pressure under the surface, which was not taken into account in our numerical model of the planar tissue-air interface. Therefore, the thresholds for comparison with BH exposures were determined from the cases where the surface was positioned outside of the transducer focal lobe (prefocally or postfocally), to minimize the effect of mound formation. Thus determined threshold peak negative pressure in the subsurface standing wave was around $P_{-} = 4$ MPa (or 2 MPa in the incident wave), which was in agreement with higher amplitude BH exposures.

In comparing the results to prior art, a 2.9 MPa atomization threshold was reported by Simon et al (2012) for an $F\#$ = 1 HIFU source focused at the surface of a porcine blood clot. The atomization threshold observed here under the same conditions for the transducer with $F\#$=1 was substantially higher. The discrepancy can be attributed to the difference in threshold criteria: in Simon et al (2012) the ejection of fine atomized tissue spray at the clot surface was observed, whereas in our work the generation of a pinhole damage to the surface visible by eye was defined as threshold, and it was observed at higher output levels than ejection of the fine spray.

The same pulse repetition rate was kept for all transducers, but since the transducer with the highest F-number ($F\#$ = 1.6) produced significantly lower saturated pressures compared to the other two sources (figure 3 (c)), longer BH pulses (20-ms) were utilized for this source compared to other ones (10-ms) to ensure BH conditions. Simon et al. (2012), however, have shown that significant atomization at tissue or water surface is typically preceded by a mound formation due to surface displacement by acoustic radiation force. Here in this work, we have estimated that tissue displacement for $F\#$ = 1.6 source reaches saturation within less than 10 ms (figure 3(d)). We, therefore, do not expect the use of longer pulses for this transducer to have any influence on the atomization threshold results.

The atomization thresholds determined in bovine clot material were then compared to those in water, as the process of acoustic atomization has been much more thoroughly investigated in prior works for water-air interface. Similarly to the clot material, the peak negative subsurface pressure causing a visible detachment of a water droplet from the surface was defined as threshold, and it was also observed to be dependent on the focus position relatively to the surface. This dependence was especially pronounced for the two transducers with lowest F-numbers, arguably due to the same reasons as in the clot model – formation of a mound with high curvature at the water surface not accounted for in the numerical model of the field. The use of the transducer with the highest F-number showed a more constant value of threshold subsurface P_-=1.1 MPa across the full range of focus locations, which is in agreement with our expectations of a threshold independent of the focus location and defined by the propagation medium properties only. This is likely due to the wider focal lobe of this source and quasi-linear incident wave that did not appreciably distort the water surface and therefore subsurface pressure level. The threshold P_- for the two other transducers also decreased to the same value of 1–1.5 MPa outside of their focal lobes. This value of approximately 0.5–0.75 MPa in the incident wave is lower than that obtained by Simon et al (2012) – 3.2 MPa – for the $F\#$ = 1 source focused at the water surface, arguably because we considered the threshold intensity as that inducing water droplet detachment as observed by the eye whereas in Simon's study the atomization criterion was the explosion of one of the droplets in an emerging drop chain which was detected by the high-speed camera at higher intensities than a single droplet detachment.

In this study, the danger zones were obtained using specific BH exposure protocols, and their outlines were, in part, related to those of volume BH lesions. As was discussed in the Introduction, variations in ultrasound frequency, pulse length, number of pulses per point or duty cycle may affect the BH lesion sizes and, therefore, danger zones. The considerations below discuss separately the potential effect of the following parameters: HIFU transducer

frequency, transducer *F*-number, pulse duration, number of pulses, duty cycle and tissue type.

1. *HIFU transducer frequency.* The ultrasound frequency of 1.5 MHz was chosen as a representative case for abdominal applications of HIFU in general and BH in particular that typically use 1–2 MHz range (Xu et al 2021, Vlaisavljevich et al 2013, 2015a, Knott et al 2019, Khokhlova et al 2011, 2016, Wang 2013). The proximity to gas-containing bodies such as intestines and lungs is also of most concern for these applications. In present study we did not explore the dependence of atomization threshold and danger zone outline on the HIFU frequency, however, Simon (2013) has found that water atomization pressure thresholds were similar within the 0.155–2 MHz range. We therefore speculate that the dependencies on pressure identified here should also be applicable to frequencies within this range.

2. *Transducer shape (or F-number).* All three transducers with different focusing angles (*F*-number from 0.83 to 1.6) tested in this study produced surface erosions contained within 4 MPa peak rarefactional pressure contour prefocally, within typical BH lesion “head” in the focal region, and within the axial and transverse pressure nulls postfocally (Fig. 8). These results allow for a generalization that the established danger zone contours are applicable for any focusing angle within this range, typical for practical applications of HIFU and BH.

3. *Number of pulses.* The number of pulses was taken to be very large here, beyond saturation of BH lesion size in any tissues explored in that context. We, therefore, believe that the use of a larger number of pulses would not produce surface damage beyond the outlines of the established danger zone; the use of fewer pulses may produce surface damage smaller than the outline of the threshold. This is one of the reasons the setup considered here is claimed to represent the worst-case scenario.

4. *Tissue type.* As hematoma represents the softest tissue model, and the easiest to liquefy compared to other tissues, it is reasonable to assume that the danger zone outlines for other tissues will be smaller than that for hematoma. This is also consistent with our definition of worst-case scenario as above.

5. *Pulse duration.* In this study, the pulse durations typical for BH were used – 10 and 20 ms. However, BH may be used with lower pulse durations within the range of 1–10 ms. As was previously shown by us and others, in both hematomas and other tissues, the resulting BH lesions (at saturation with respect to number of pulses) are either the same size or smaller than with longer pulse durations (Khokhlova et al 2016, 2017, Ponomarchuk et al 2021). Thus, the damage threshold outline may also be expected to be tighter than those identified in this work for those longer pulses. In the case of even longer pulses than considered in this study (e.g., 30–100 ms) the spatial extent of mechanical damage is expected to be similar to that with shorter pulses (as shown for example in Khokhlova et al. 2013, 2014), however, the thermal effects are expected to be more significant,

which may have a confounding effect. Thus, for pulses longer than 20 ms the damage threshold is likely to be different than what is reported here.

6. *Duty cycle.* The duty cycles of 1–2% used here are typical for BH exposures where thermal effects are to be avoided. At duty cycles of 5% and higher, thermal effects are expected to be substantially more pronounced (Wang et al 2018), and the damage to tissue, as well as any air-tissue boundary, will contain a mix of thermal and mechanical effects. Thus, the damage thresholds defined here are only applicable to low duty cycles, e.g., 1–2%, which produce mechanical damage only.

In case of non-histotripsy exposures using pulsed HIFU fields without initiation of cavitation or boiling, we hypothesize the danger zone outlines would follow the 4 MPa peak negative pressure contour in the standing wave, or 4 MPa peak-to-peak pressure in the incident field. This means, in case of any damage to the surface, the surface erosion would have a circular (or elliptical, in case of non-orthogonal incidence) shape not exceeding the 4 MPa contour cross-section in diameter.

It is important to note that the goal of this study was to establish the threshold pressure *in situ* to be avoided during BH treatment near the air boundary rather than to predict the size of the surface erosion if it was to occur. The danger zone contours established in this work, therefore, do not outline the resulting lesion but rather identify the “danger volume”, within which the tissue-air boundaries should not be present to avoid damage.

One limitation of the current study is that the tissue-air interface was planar and orthogonal to the incident HIFU beam, whereas this may not be a common scenario in practical clinical situations. In such cases of oblique beam incidence onto tissue-air interface, the constructive interference of the reflected and incident waves would be less efficient, thus the peak pressures in the forming standing wave would be lower than the peak-to-peak pressure within the incident wave. Accordingly, the zone of potential damage will be smaller than what would be estimated based on the damage threshold established here – 4 MPa peak-to-peak pressure in the incident wave. As such, the setup considered in this study represents the worst-case scenario in terms of incidence angle onto the tissue-air boundary.

Another limitation of the results obtained in the present study is a critical effect of tissue inhomogeneities in the acoustic propagation path that occurs in clinical settings and leads to the beam aberration and refraction. Sufficient *in situ* shock amplitude (and hence focal pressures) at the focus needs to be reached for BH to be feasible. In practice, as a step of treatment planning, the sufficient acoustic power is determined before each treatment by gradually increasing the output power and depositing isolated BH pulses at the focus until bubble activity (hyperechoic region on ultrasound imaging) is detected. The appearance of that hyperechoic region indicates that the required shock amplitude has been reached *in situ*. Thus, this treatment planning procedure also serves for evaluation of focal *in situ* pressures. Once the focal *in situ* pressure is known, the iso-pressure contour of 4 MPa (corresponding to the danger zone outline) may be predicted assuming that the HIFU beam has maintained its free-field shape. The actual HIFU beam is, however, frequently deformed by aberration induced by soft tissue layers, in some cases hindering any treatment initiation, even at the

highest output level (Thomas et al 2022). In those cases, the danger zone evaluated as above is unlikely to be reliable, and should only be used if the degree of aberration is deemed to be low, which can be predicted using procedures recently described by others (Thomas et al 2022, Yeats et al 2022).

We believe the results obtained in this work are practically relevant for future clinical applications of boiling histotripsy. We imagine the acoustic field *in situ* would be predicted numerically based on preoperative CT scans (Gu and Jing 2015), and the danger zone could be outlined based on the threshold pressures obtained in this work. The danger zone contours could then be superimposed onto real-time imaging and used for targeting to avoid critical gas-containing structures surrounding the treatment site.

5. Conclusion

One of the key aspects crucial to the introduction of the BH methods into clinical use in abdominal targets is identifying practical guidelines to ensure safe treatments in proximity to gas-containing organs. Here we have shown that the area of BH-induced mechanical damage to tissue-air interface can be correlated to the spatial distribution of peak-to-peak pressure in the incident wave. These pressure-based danger zones can be superimposed onto in-treatment ultrasound images during BH of soft tissues, and gas-containing organ surfaces should be located outside those margins to avoid mechanical damage. These danger zone outlines were obtained in a very soft and fragile biomaterial – blood clot – and therefore represent the most conservative recommendations with regards to any soft tissues.

Acknowledgements

This work was supported in part by NIH R01GM122859, RFBR 20-02-00210 grants, Interdisciplinary Scientific and Educational School of Moscow University «Photonic and Quantum technologies. Digital medicine», and “BASIS” Foundation student grant 20-2-10-10-1.

References

[1]. Aikawa T, Nobuki K 2021 Relation between thresholds of free radical generation and atomization under ultrasound exposure Jpn J Appl Phys 60 SDDD13

[2]. Andreev VG, Dmitriev VN, Pishchalnikov YA, Rudenko OV, Sapozhnikov OA, Sarvazyan AP 1997 Observation of shear waves excited by focused ultrasound in a rubber-like medium Acoust Phys 43 123–128

[3]. Canney MS, Khokhlova VA, Bessonova OV, Bailey MR, Crum LA 2010 Shock-induced heating and millisecond boiling in gels and tissue due to high intensity focused ultrasound Ultrasound Med Biol 36 250–267 [PubMed: 20018433]

[4]. Canney M S, Bailey MR, Crum LA, Khokhlova VA, Sapozhnikov OA 2008 Acoustic characterization of high intensity focused ultrasound fields: A combined measurement and modeling approach J Acoust Soc Am 124 2406–2420 [PubMed: 19062878]

[5]. Duck F 1990 Physical properties of tissue: A comprehensive reference book London: Academic Press

[6]. Gaete-Garretón L, Briceño-Gutiérrez D, Vargas-Hernández Y, Zanelli CI 2018 Ultrasonic atomization of distilled water J Acoust Soc Am 144 222–227 [PubMed: 30075687]

[7]. Grybauskas P, Kundrotas K, Sukackas V, Yaronis E 1978 Ultrasonic digital interferometer for investigation of blood clotting Ultrasonics 16 33–36 [PubMed: 622750]

[8]. Gu J, Jing Y 2015 Modeling of wave propagation for medical ultrasound: a review IEEE Trans Ultrason Ferroelectr Freq Control 62 1979–1992 [PubMed: 26559627]

[9]. Hunter C, Sapozhnikov OA, Maxwell AD, Khokhlova VA, Wang YN, MacConaghy B, Kreider W 2016 An ultrasonic caliper device for measuring acoustic nonlinearity Phys Procedia 87 93–98 [PubMed: 28616100]

[10]. Khokhlova TD, Canney MS, Khokhlova VA, Sapozhnikov OA, Crum LA, Bailey MR 2011 Controlled tissue emulsification produced by high intensity focused ultrasound shock waves and millisecond boiling J Acoust Soc Am 130 3498–3510 [PubMed: 22088025]

[11]. Khokhlova TD, Haider YA, Maxwell AD, Kreider W, Bailey MR, Khokhlova VA 2017 Dependence of boiling histotripsy treatment efficiency on HIFU frequency and focal pressure levels Ultrasound Med Biol 43 1975–1985 [PubMed: 28641910]

[12]. Khokhlova TD, Kucewicz JC, Ponomarchuk EM, Hunter C, Bruce M, Khokhlova VA, Matula TJ, Monsky W 2020 Effect of stiffness of large extravascular hematomas on their susceptibility to boiling histotripsy liquefaction in vitro // Ultrasound Med Biol 46 2007–2016 [PubMed: 32444137]

[13]. Khokhlova TD, Monsky WL, Haider YA, Maxwell A, Wang Y-N, Matula TJ 2016 Histotripsy liquefaction of large hematomas Ultrasound Med Biol 42 1491–1498 [PubMed: 27126244]

[14]. Khokhlova TD, Wang YN, Simon JC, Cunitz BW, Starr F, Paun M, Crum LA, Bailey MR, Khokhlova VA 2014 Ultrasound-guided tissue fractionation by high intensity focused ultrasound in an in vivo porcine liver model PNAS 111 8161–8166 [PubMed: 24843132]

[15]. Khokhlova T, Kuzcevic J, Hunter C, Maxwell A, Khokhlova V, Matula T, Monsky W 2018a Boiling histotripsy liquefaction of large extravascular hematomas: in vitro optimization and device design considerations Abstract book of the 6th International Symposium on Focused Ultrasound 151–152.

[16]. Khokhlova T, Rosnitskiy P, Hunter C, Maxwell A, Kreider W, Ter Haar G, Costa M, Sapozhnikov O, Khokhlova V 2018b Dependence of inertial cavitation induced by high intensity focused ultrasound on transducer F-number and nonlinear waveform distortion. J Acoust Soc Am 144 1160 [PubMed: 30424663]

[17]. Khokhlova VA et al. 2015 Histotripsy methods in mechanical disintegration of tissue: towards clinical applications Int. J. Hyperthermia 31 145–62 [PubMed: 25707817]

[18]. Khokhlova VA, Yuldashev PV, Mezdrokhin I, Rosnitskiy P, Karzova MM, Kreider W, Sapozhnikov O 2018 Development of a freely available simulator with graphical interface for modeling nonlinear focused ultrasound fields with shocks. J Acoust Soc Am 144 1699

[19]. Kim G, Cheng S, Hong L, Kim JT, Li KC, Chamorro LP 2021 On the acoustic fountain types and flow induced with focused ultrasound J Fluid Mech 909 R2

[20]. Knott EA, Swietlik JF, Longo KC, Watson RF, Green CM, Abel EJ, Lubner MG, Hinshaw JL, Smolock AR, Xu Z, Lee FT Jr, Ziemlewicz TJ 2019 Robotically-assisted sonic therapy for renal ablation in a live porcine model: initial preclinical results J Vasc Interv Radiol 30 1293–1302 [PubMed: 31130365]

[21]. Li JJ, Xu GL, Gu MF, Luo GY, Rong Z, Wu PH, Xia JC 2007 Complications of high intensity focused ultrasound in patients with recurrent and metastatic abdominal tumors World J Gastroenterol 13 2747–2751 [PubMed: 17569147]

[22]. Matula TJ, et al. 2021 Treating porcine abscesses with histotripsy: a pilot study Ultrasound Med Biol 47 603–61 [PubMed: 33250219]

[23]. Maxwell AD et al. 2017 A prototype therapy system for transcutaneous application of boiling histotripsy IEEE Trans Ultrason Ferroelectr Freq Control 64 1542–155 [PubMed: 28809681]

[24]. Maxwell A, Sapozhnikov O, Bailey M, Crum L, Xu Z, Fowlkes B, Cain C, Khokhlova V 2012. Disintegration of tissue using high intensity focused ultrasound: Two approaches that utilize shock waves Acoustics Today 8 24–36

[25]. Nahirnyak VM, Yoon SW, Holland CK 2006 Acoustomechanical and thermal properties of clotted blood J Acoust Soc Am 119 3766–3772 [PubMed: 16838520]

[26]. Pahk KJ, de Andrade M O, Gélat P, Kim H, Saffari N 2019 Mechanical damage induced by the appearance of rectified bubble growth in a viscoelastic medium during boiling histotripsy exposure Ultrason Sonochem 53 164–177 [PubMed: 30686603]

[27]. Pahk KJ, Lee S, Gélat P, de Andrade M O, Saffari N 2021 The interaction of shockwaves with a vapour bubble in boiling histotripsy: The shock scattering effect Ultrason Sonochem 70 105312 [PubMed: 32866882]

[28]. Pierce AD 2014 Basic linear acoustics In Springer Handbook of Acoustics New York: Springer 2nd edition 89

[29]. Pishchalnikov YA, Sapozhnikov OA, Sinilo TV 2002 Increase in the efficiency of the shear wave generation in gelatin due to the nonlinear absorption of a focused ultrasonic beam Acoust Phys 48 214–219

[30]. Poliachik SL, Khokhlova TD, Wang YN, Simon JC, Bailey MR 2014 Pulsed focused ultrasound treatment of muscle mitigates paralysis-induced bone loss in the adjacent bone: a study in a mouse model Ultrasound Med Biol 40 2113–2124 [PubMed: 24857416]

[31]. Ponomarchuk EM et al. 2021 Ultrastructural analysis of volumetric histotripsy bio-effects in large human hematomas Ultrasound Med Biol 47 2608–2621 [PubMed: 34116880]

[32]. Prieur F, Sapozhnikov OA 2017 Modeling of the acoustic radiation force in elastography J Acoust Soc Am 142 947–961 [PubMed: 28863603]

[33]. Rozenberg LD, Eknadiosyants OK 1960 Kinetics of ultrasonic fog formation Sov Phys Acoust 6 369–374

[34]. Sapozhnikov OA High-intensity ultrasonic waves in fluids: Nonlinear propagation and effects 2015 Applications of High-intensity Ultrasound Power Ultrasonics 66 9–35

[35]. Simon J 2014 The thresholds and mechanisms of tissue injury by focused ultrasound Doctoral dissertation

[36]. Simon JC, Sapozhnikov OA, Khokhlova VA, Crum LA, Bailey MR 2015 Ultrasonic atomization of liquids in drop-chain acoustic fountains J Fluid Mech 766 129–146 [PubMed: 25977591]

[37]. Simon JC, Sapozhnikov OA, Khokhlova VA, Wang Y-N, Crum LA, Bailey MR 2012 Ultrasonic atomization of tissue and its role in tissue fractionation by high intensity focused ultrasound Phys Med Biol 57 8061–8078 [PubMed: 23159812]

[38]. Thomas GPL, Khokhlova TD, Sapozhnikov OA, Wang YN, Totten S, Khokhlova VA 2022 In vivo aberration correction for transcutaneous HIFU therapy using a multi-element array IEEE Trans Ultrason Ferroelectr Freq Control

[39]. Tomita Y 2014 Jet atomization and cavitation induced by interactions between focused ultrasound and a water surface Phys. Fluids 26 097105

[40]. Vlaisavljevich E, Gerhardson T, Hall T, Xu Z 2017 Effects of f-number on the histotripsy intrinsic threshold and cavitation bubble cloud behavior Phys Med Biol 62 1269–1290 [PubMed: 27995900]

[41]. Vlaisavljevich E, Kim Y, Allen S, Owens G, Pelletier S, Cain C, Ives K, Xu Z 2013 Image-guided non-invasive ultrasound liver ablation using histotripsy: feasibility study in an in vivo porcine model Ultrasound Med Biol 39 1398–1409 [PubMed: 23683406]

[42]. Vlaisavljevich E, Kim Y, Owens G, Roberts W, Cain C, Xu Z 2014 Effects of tissue mechanical properties on susceptibility to histotripsy-induced tissue damage Phys Med Biol 59 253–270 [PubMed: 24351722]

[43]. Vlaisavljevich E, Lin KW, Maxwell A, Warnez MT, Mancia L, Singh R, Putnam AJ, Fowlkes B, Johnsen E, Cain C, Xu Z 2015a Effects of ultrasound frequency and tissue stiffness on the histotripsy intrinsic threshold for cavitation Ultrasound Med Biol 41 1651–1667 [PubMed: 25766571]

[44]. Vlaisavljevich E, Lin KW, Warnez MT, Singh R, Mancia L, Putnam AJ, Johnsen E, Cain C, Xu Z 2015b Effects of tissue stiffness, ultrasound frequency, and pressure on histotripsy-induced cavitation bubble behavior Phys Med Biol 60 2271–2292 [PubMed: 25715732]

[45]. Wang YN, Khokhlova TD, Bailey MR, Hwang JH, Khokhlova VA 2013 Histological and biochemical analysis of mechanical and thermal bioeffects in boiling histotripsy lesions induced by high intensity focused ultrasound Ultrasound Med Biol 39 424–438 [PubMed: 23312958]

[46]. Wang YN, Khokhlova TD, Buravkov S, Chernikov V, Kreider W, Partanen A, Farr N, Maxwell A, Schade GR, Khokhlova VA 2018 Mechanical decellularization of tissue volumes using boiling histotripsy Phys Med Biol 63 1–11

[47]. Waters NE 1965 The indentation of thin rubber sheets by spherical indentors Br J Appl Phys 16 557–563

[48]. Xu Z, Hall TL, Vlaisavljevich E, Lee FT Jr 2021 Histotripsy: the first noninvasive, non-ionizing, non-thermal ablation technique based on ultrasound Int J Hyperthermia 38 561–575 [PubMed: 33827375]

[49]. Yeats E, Gupta D, Xu Z, Hall TL 2022 Effects of phase aberration on transabdominal focusing for a large aperture, low *f*-number histotripsy transducer Phys Med Biol 67

[50]. Yuldashev PV, Karzova MM, Kreider W, Rosnitskiy PB, Sapozhnikov OA, Khokhlova VA 2021 "HIFU beam:" a simulator for predicting axially symmetric nonlinear acoustic fields generated by focused transducers in a layered medium IEEE Trans Ultrason Ferroelectr Freq Control 68 2837–2852 [PubMed: 33877971]

[51]. Yuldashev PV, Mezdrokhin IS, Khokhlova VA 2018 Wide-angle parabolic approximation for modeling high-intensity fields from strongly focused ultrasound transducers Acoust Phys 64 309–319

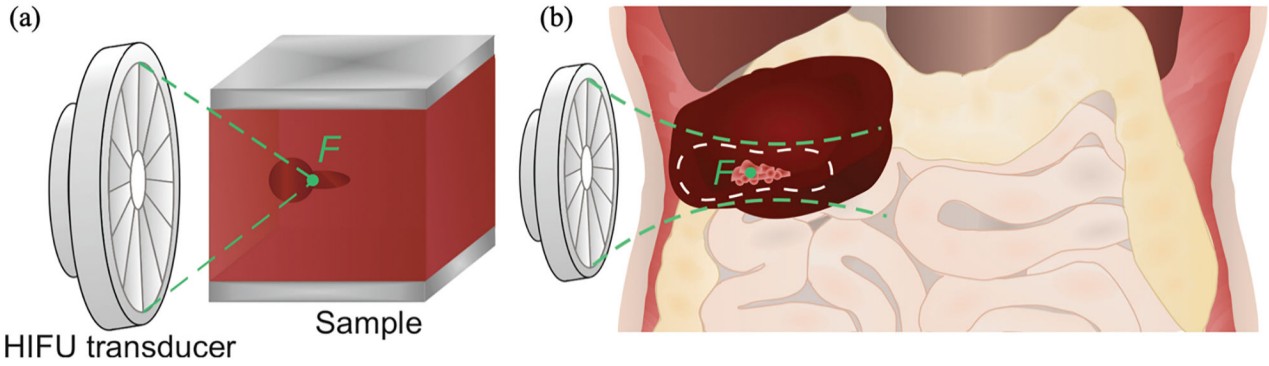

Figure 1.

(a) Schematic of a typical BH lesion shape induced in a bulk of soft tissue. (b) Schematic illustration of the BH lesion induced in a hematoma close to gas-containing organs (intestines) and the danger zone outline (white dashed contour) around the HIFU focus *F* (green point).

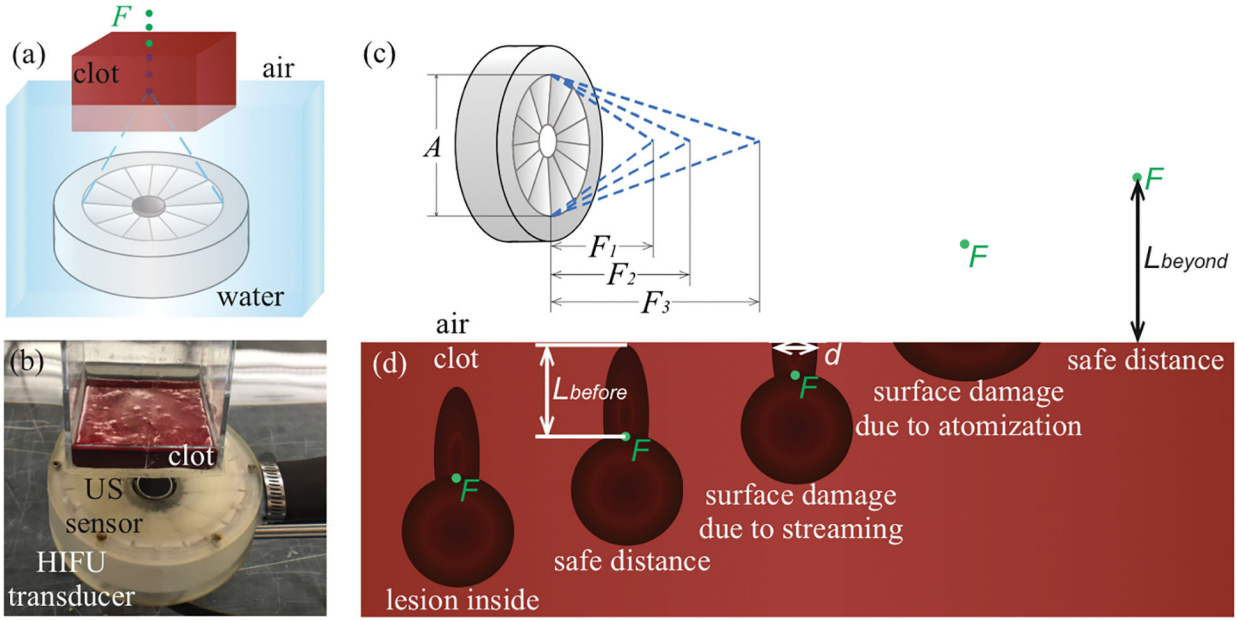

Figure 2.

A schematic (a) and a photograph (b) of the experimental setup for the study of thresholds for mechanical damage of clot-air interface. (c) Schematic illustration of the three focusing angles used. (d) Illustration of the damage induced in the hematoma with the focus F (green point) near the clot-air interface. L_{before} – safe distance for focus before the surface, L_{beyond} – safe distance for focus beyond the surface, d – surface damage diameter.

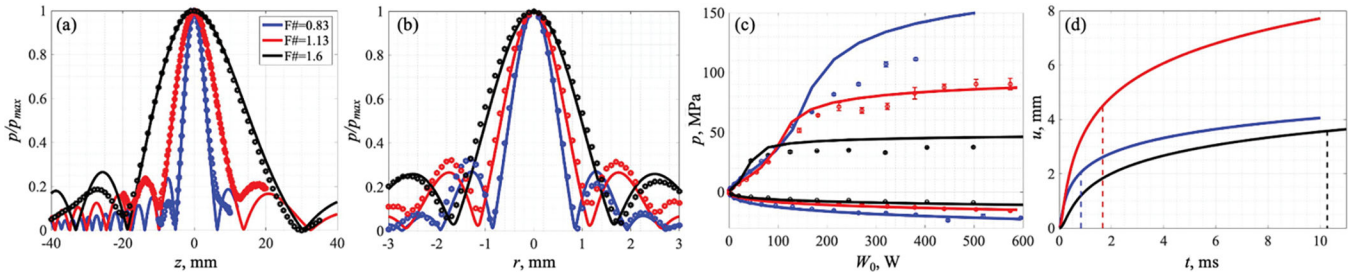

Figure 3.

(a,b) Normalized axial (a) and transverse (b) pressure amplitude distributions in a linear beam in water measured by the capsule hydrophone (symbols) and numerically simulated (solid lines) based on the equivalent source method. (c) Experimental (symbols) and theoretical (solid lines) saturation curves of peak positive and negative focal pressures in dependence on the source output power W_0. (d) Theoretical evaluation of tissue displacement over exposure time (solid lines) induced by the radiation force of the HIFU beam focused inside the clot. Dashed lines correspond to the evaluated time of boiling initiation. Transducer with $F\#$ = 0.83 is represented by the blue line, $F\#$ = 1.13 by the red line and $F\#$ = 1.6 by the black line.

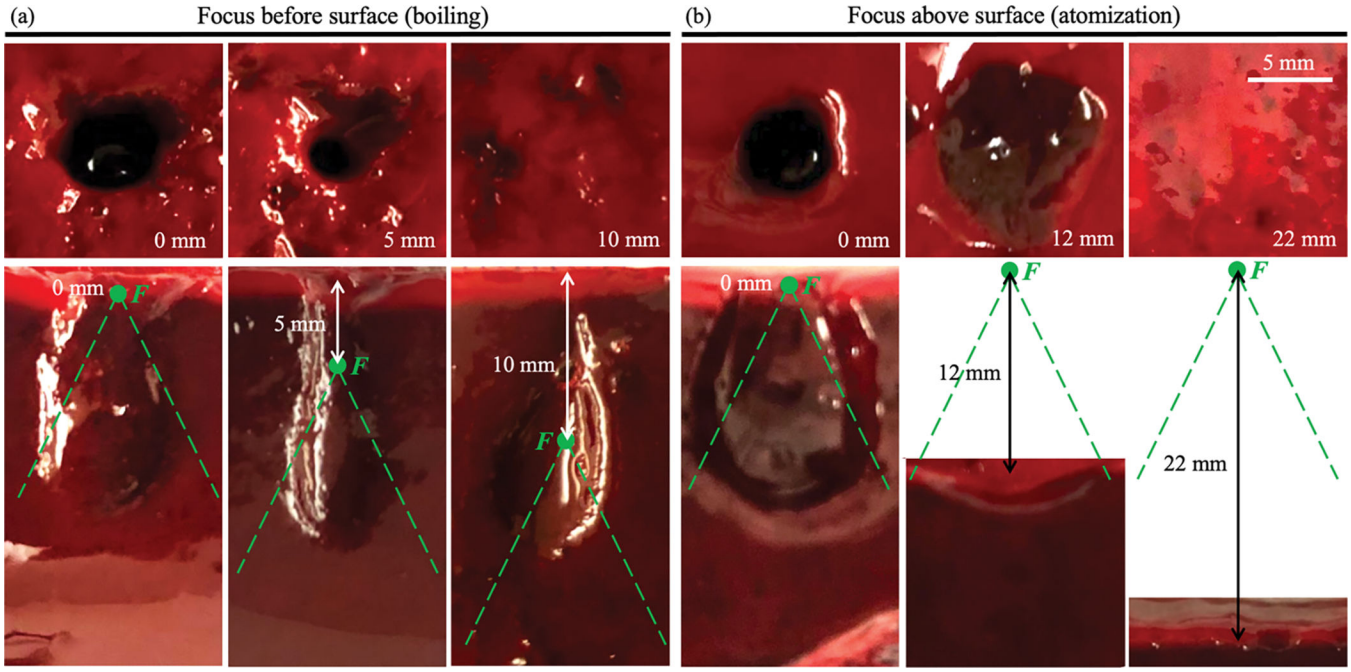

Figure 4.

Illustration of the change in surface erosion diameter (top row) and lesion shape in axial plane (bottom row) with distance between the focus F (green point) and the clot-air interface for the transducer with $F\#$ = 1.13. (a) Focus positioned at the surface (left column), 5 mm before the surface (middle column), at a safe distance L_{before} – 10 mm before the surface (right column). (b) Focus positioned at the surface (left column), 12 mm beyond the surface (middle column), at a safe distance L_{beyond} – 22 mm beyond the surface (right column). Dashed green lines indicate HIFU beam geometry. HIFU incident towards the observer (top row) or from the bottom of the image (bottom row). Scale bar – 5 mm.

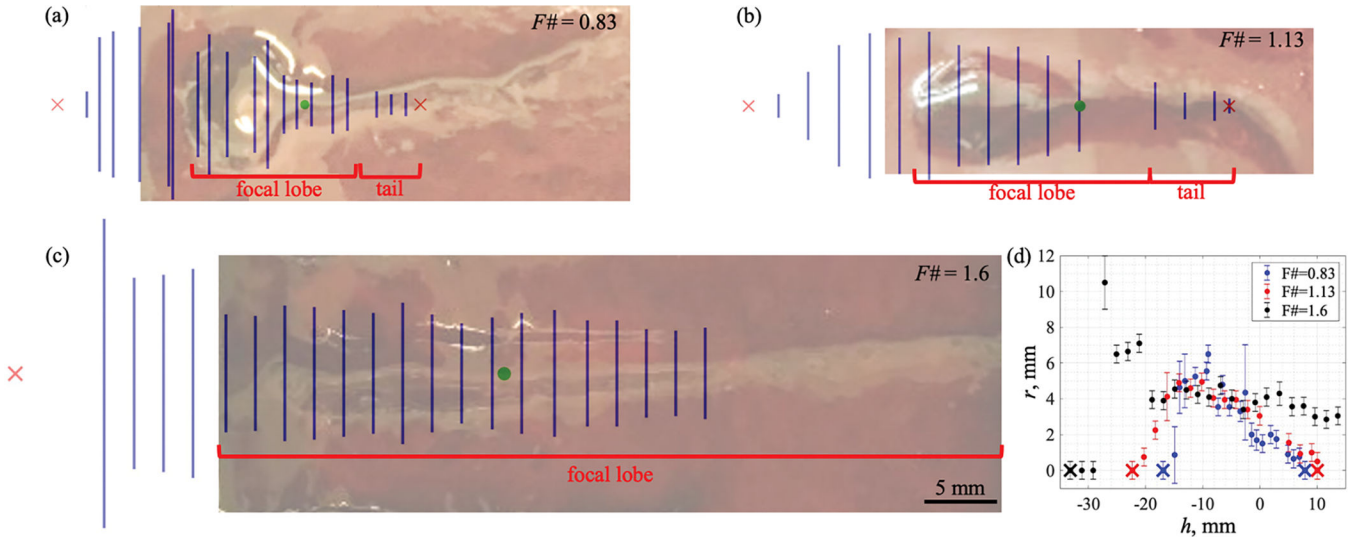

Figure 5.

(a–c) Average diameters of the erosion at the surface (blue vertical lines, indicating diameter *d* from figure 2(d)) positioned at varying distances from the focus (green point) superimposed onto photographs of typical BH lesions induced in hematoma far from its boundaries. Red crosses indicate safe distances between the focus and the surface. HIFU incident from the left. Scale bar – 5 mm. The danger zone outline is positioned more prefocally and less postfocally compared to the shape of a typical in-bulk BH lesion. (d) Average radii of the surface damage *vs* focus–interface distance: focus positioned *h* mm before ($h<0$) or beyond ($h>0$) the clot surface. Transducer with *F#* = 0.83 is represented by the blue markers, with *F#* = 1.13 by the red markers, and with *F#* = 1.6 by the black markers. Crosses indicate safe distances between the focus and the surface. Error bars show combined standard deviations and instrument uncertainties of a ruler.

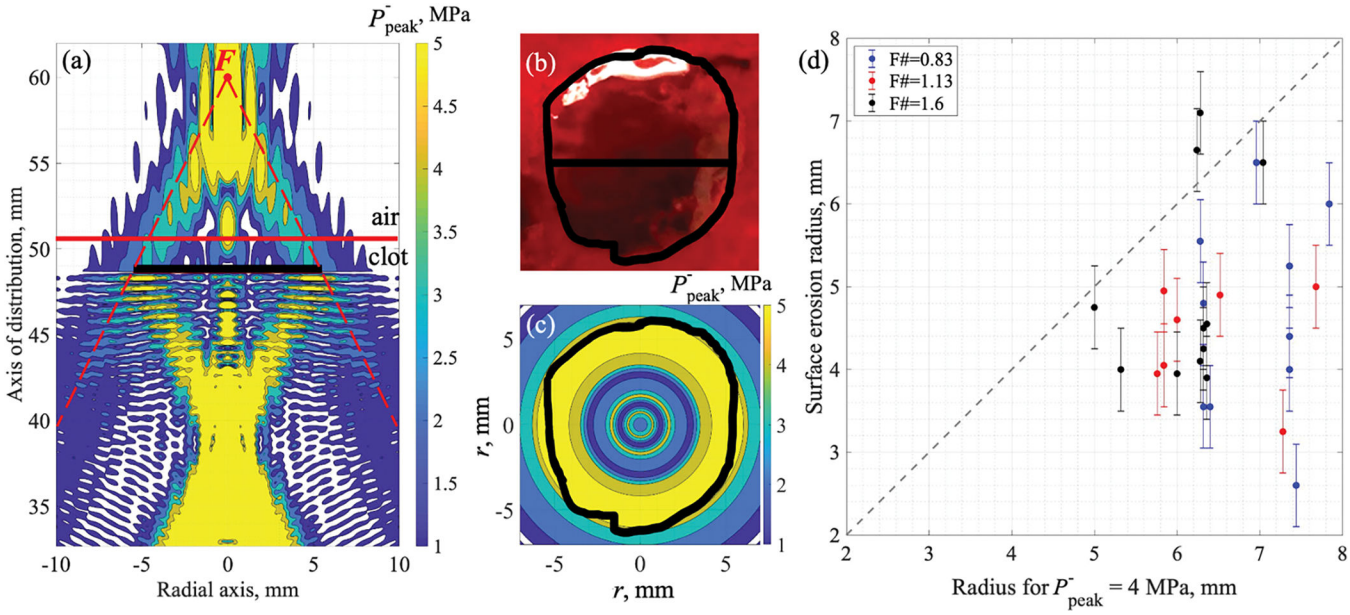

Figure 6.

Surface damage correlation with the peak negative pressure field geometry in the standing wave: (a–c) for *F#* = 0.83 transducer with focus *F* (red point) positioned 10 mm beyond the clot-air interface; and (d) for all tranducers at different focus-surface distances. (a) Calculated peak negative pressure contours of 1, 2, 3, 4 and 5 MPa in the axial plane with the projection of the corresponding surface damage (black solid line). Dashed red lines indicate HIFU beam geometry. (b) Diameter and an outline of the surface damage (black solid lines) superimposed onto its gross photograph. (c) Surface damage outline (black solid line) superimposed onto peak negative pressure contours of 1, 2, 3, 4 and 5 MPa in the maximum P_- lateral distribution calculated within λ/4-thick layer under the bottom of the lesion. HIFU is incident from the bottom (a) or towards the observer (b, c). Scale is the same for (a–c). (d) Surface erosion diameters obtained with focus positioned beyond the clot-air interface *vs* radii of the 4 MPa peak negative pressure contour in the maximum P_- lateral distribution calculated within λ/4-thick layer under the bottom of the lesion. Dashed gray line indicates the identity line.

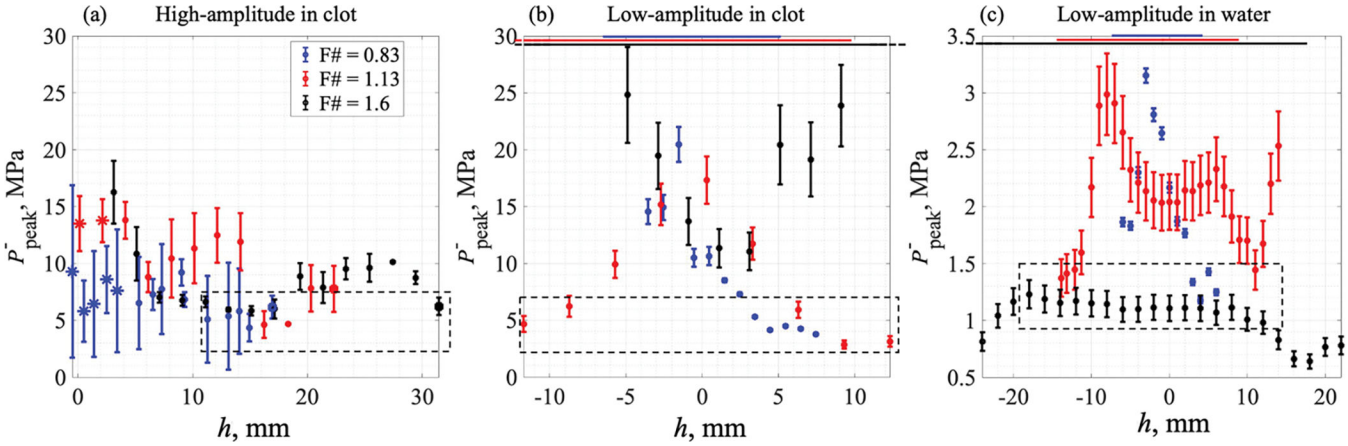

Figure 7.

Maximum negative pressures in standing wave: under BH lesion bottom (a) and under clot-air (b) or water-air (c) boundary at a threshold intensity. (a) Maximum amplitude of the peak negative pressure in a standing wave in a cylindrical λ/4-thick layer with the surface damage radius under the BH-induced lesion bottom. Focus was positioned beyond the clot surface (h>0). Asterisk markers indicate boiling-induced lesions; filled square markers indicate focus being positioned at a safe distance from the clot-air interface; circle markers indicate atomization-induced lesions. Dashed rectangular contour in (a) outlines the lowest P_- values causing damage to the hematoma surface over the entirety of focus positions. (b) Maximum amplitude of the peak negative pressure in a standing wave in a 2λ-thick layer under the clot-air interface at a threshold intensity resulting in a pinhole generation at the clot surface. (c) Maximum amplitude of peak negative pressure in a standing wave in a 2λ-thick layer under the water-air interface at a threshold intensity resulting in a water droplet detachment. In (b) and (c), focus was positioned h mm before (h<0) or beyond (h>0) the clot surface, and the horizontal lines at the top indicate the axial dimensions of the focal lobe for the corresponding transducers. Dashed rectangular contours in (b,c) outline the data points for focus positioned at the edge of or outside the focal lobe. Transducer with F# = 0.83 is represented by the blue line, F# = 1.13 by the red line and F# = 1.6 by the black line.

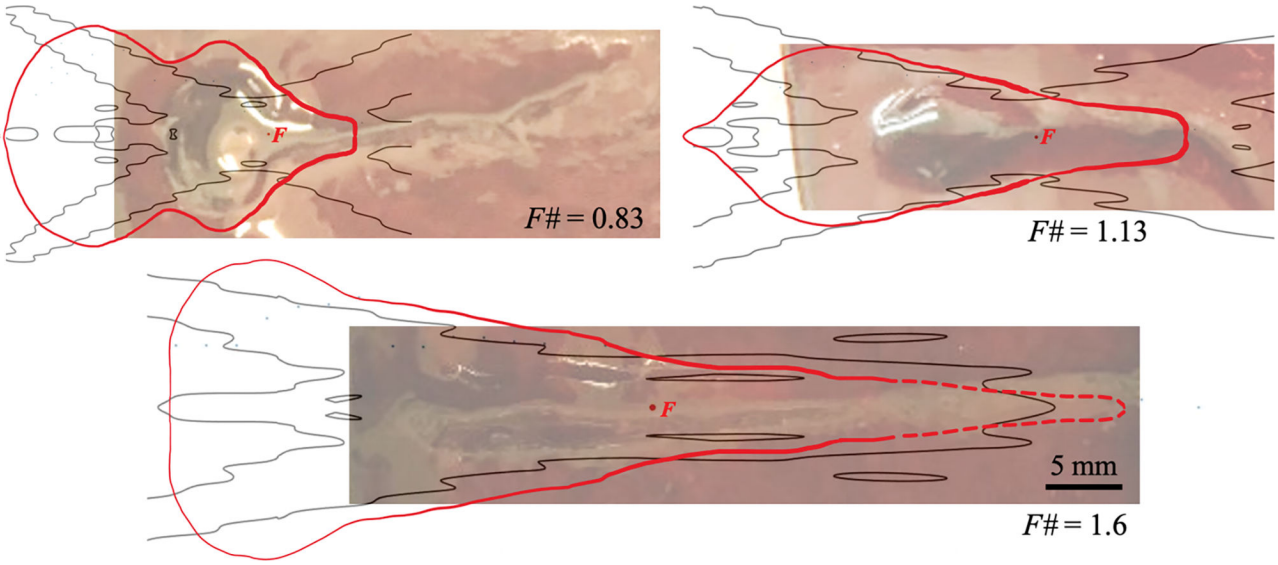

Figure 8.

Danger zone outlines (red line) for air-boundary around a BH-focus *F* (red point) superimposed onto photographs of typical BH lesions and the contours of 4 MPa peak-to-peak pressure in the incident acoustic field (black line). The dashed line for *F*#=1.6 transducer indicates assumed danger zone outline based on the results for other two transducers. HIFU incident from the left. Scale bar – 5 mm.

Table 1.

Transducer nominal parameters and corresponding pulsing protocols for interface damage threshold determination

F#	0.77	1.02	1.51
f_0	1.5 MHz	1.5 MHz	1.5 MHz
α	81°	58°	39°
V	110 V	130 V	180 V
W_0	320 W	442 W	404 W
t_{pulse}	10 ms	10 ms	20 ms
N_p	30	30	30
DC	1%	1%	2%
In situ $P_+ / P_- / As$	134.4 / −19.33 / 119 MPa	87.17 / −14 / 95.3 MPa	44 / −8.624 / 51.52 MPa
t_b, ms	0.8	1.66	10.3
I_{sppa}	43.7 kW/cm^2	24.8 kW/cm^2	8 kW/cm^2

F# = nominal *F*-number; f_0 = operational ultrasound frequency; α = nominal focusing angle; V = source output voltage; W_0 = acoustic output power *in situ*; t_{pulse} = pulse duration; N_p = number of pulses per sonication point; $P_+(P_-)$ = peak positive (negative) pressure at the focus at the average depth *in situ*; A_S = focal shock amplitude *in situ*; t_b = time to boil; I_{sppa} = spatial-peak pulse-average intensity at the average depth *in situ*.

Table 2.

HIFU transducers nominal geometric parameters and the corresponding equivalent source parameters used in numerical simulations

	Highly focusing		Medium focusing		Weakly focusing	
	Nominal	**Effective**	**Nominal**	**Effective**	**Nominal**	**Effective**
F, mm	56.4	60	76.8	80	118.1	120
A, mm	73	72.7	75	71	78	75
O, mm	24	30	24	30	24	30
F#	0.77	0.83	1.02	1.13	1.51	1.6
S, cm^2	42.92	39.05	42.63	34.63	44.63	38.22
p_0/V, kPa/V	4.508		4.76		3.128	

F = focal distance; *A* = aperture; *O* = central opening diameter; *F*# = *F*-number; *S* = source surface area; p_0 = pressure amplitude on the transducer; *V* = output voltage.

Table 3.

Comparison of the lesion dimensions with characteristic parameters of the simulated incident linear pressure field

F#	L_{before}, mm	Δz_{post}, mm	L_{beyond}, mm	<*l*>, mm	Δz_{pre}, mm	<*d*>, mm	<*D*>, mm	Δr, mm
0.83	7	6.45	18	8.2±0.8	5.25	1.5±0.2	1.8±0.5	1.7
1.13	10	13.8	22	10.1±1.3	9.9	2.41±1.03	2.1±0.5	2.3
1.6	>16	30.5	30	22.5±0.7	18.7	5.7±0.5	3.1±1.1	3.34

L_{before} = safe distance for focus before the surface; Δz_{post} = distance from focus to the first postfocal pressure axial null; L_{beyond} = safe distance for focus beyond the surface; <*l*> = average length of the BH lesion “head” when focus was before the surface; Δz_{pre} = distance from the first prefocal pressure axial null to focus; <*d*> = average diameter of the surface erosion when focus was inside the clot with the surface outside the focal lobe; <*D*> = average diameter of the BH lesion “tail” when focus was positioned before the surface; Δr = focal lobe width at the nulls.